Frequency-dependent complex modulus of the uterus: preliminary results

Miklos Z Kiss[1]**, Maritza A Hobson**[1]**, Tomy Varghese**[1,2]**, Josephine Harter**[3]**, Mark A Kliewer**[4]**, Ellen M Hartenbach**[5] **and James A Zagzebski**[1,4,6]

[1] Department of Medical Physics, University of Wisconsin, Madison, WI 53706, USA
[2] Department of Biomedical Engineering, University of Wisconsin, Madison, WI 53706, USA
[3] Department of Surgical Pathology, University of Wisconsin, Madison, WI 53706, USA
[4] Department of Radiology, University of Wisconsin, Madison, WI 53706, USA
[5] Department of Obstetrics and Gynecology, University of Wisconsin, Madison, WI 53706, USA
[6] Department of Human Oncology, University of Wisconsin, Madison, WI 53706, USA

E-mail: mzkiss@wisc.edu

Abstract

The frequency-dependent complex moduli of human uterine tissue have been characterized. Quantification of the modulus is required for developing uterine ultrasound elastography as a viable imaging modality for diagnosing and monitoring causes for abnormal uterine bleeding and enlargement, as well assessing the integrity of uterine and cervical tissue. The complex modulus was measured in samples from hysterectomies of 24 patients ranging in age from 31 to 79 years. Measurements were done under small compressions of either 1 or 2%, at low pre-compression values (either 1 or 2%), and over a frequency range of 0.1–100 Hz. Modulus values of cervical tissue monotonically increased from approximately 30–90 kPa over the frequency range. Normal uterine tissue possessed modulus values over the same range, while leiomyomas, or uterine fibroids, exhibited values ranging from approximately 60–220 kPa.

(Some figures in this article are in colour only in the electronic version)

1. Introduction

Dysfunctional uterine bleeding is the most common symptom requiring a pelvic ultrasound in women (Davidson and Dubinsky 2003, Williams *et al* 2003). In premenopausal women, common causes of dysfunctional bleeding include leiomyomas (uterine fibroids) (Kliewer *et al* 1995, Caoili *et al* 2000, Bhatia and Singh 2001) and adenomyosis (Williams *et al* 2003). For postmenopausal women, uterine bleeding could be caused by endometrial polyps, endometrial cancer, endometrial hyperplasia (or atrophy) or leiomyomas (Williams *et al* 2003). Leiomyomas and adenomyosis are common benign myometrial conditions in premenopausal

women, and present with the same clinical symptoms. Traditional treatments of these two conditions differ, however, which makes the correct and accurate diagnosis crucial (Ascher *et al* 2003).

Adenomyosis is characterized by the presence of heterotopic endometrial glands and stroma in the myometrium with adjacent smooth muscle hyperplasia, whereas leiomyomas are fibrous ingrowths into the myometrium (Reinhold *et al* 1999). Submucosal leiomyomas, or benign uterine fibroids, are growths of bundles of smooth muscle cells of the myometrium enclosed by peripheral fibres that are differentiated from normal myometrium by a capsule (Wood 1998, Bhatia and Singh 2001, Williams *et al* 2003). Leiomyomas range in size from micro- to macroscopic, and while single fibroids may be present, several of these masses are generally found at the same time in the uterus. Leiomyomas are typically benign, but can torse, infarct and impede vaginal delivery during childbirth. The current clinical treatment of leiomyomas is hysterectomy or myomectomy, drug therapy or uterine artery embolization (Keshavarzi *et al* 2001). Uterus conserving therapy is well established for women with symptomatic leiomyomas, but total hysterectomy is the treatment for debilitating adenomyosis (Ascher *et al* 2003).

Dilation and curettage is a commonly used technique for diagnosing endometrial cancer, and thus, has been the method of choice for the diagnosis of the causes of irregular uterine bleeding. However, using this method it is difficult to establish the presence of other causes of irregular uterine bleeding, such as endometrial polyps, adenomyosis or leiomyomas (Bree *et al* 2000). Hysteroscopy, a 'gold standard' for diagnosing between benign and malignant tissue because it enables clinicians to 'perform directed biopsy', is uncomfortable for the patient and requires anaesthesia (Davidson and Dubinsky 2003). Therefore, noninvasive techniques, such as ultrasound or magnetic resonance imaging (MRI), are desirable for clinical diagnosis to prevent unnecessary hysterectomies. MRI T2-weighted images are currently the most accurate imaging modality for identifying and differentiating leiomyomas from adenomyosis (Ascher *et al* 2003, Williams *et al* 2003, Berridge and Winter 2004). In contrast, ultrasound images of leiomyomas, adenomyosis and endometrial polyps, overgrowths of endometrial tissue, can all have a similar appearance, complicating their distinction (Devlieger *et al* 2003, Williams *et al* 2003, Takeuchi *et al* 2005). Comparisons of MRI and endovaginal ultrasound with histopathological detection of adenomyosis (Reinhold *et al* 1996, Bazot *et al* 2001) found that while endovaginal ultrasound was comparable to MRI in imaging of the uterine cavity, MRI was superior in detecting adenomyosis and submucosal leiomyomas. Thus, MRI is usually used for follow-up when ultrasound results are inconclusive.

Since irregular uterine bleeding is a common problem, a less expensive and more readily available alternative method to the current imaging 'gold standard', MRI, is desirable. Ultrasound elastography is a good candidate because it has already demonstrated its potential to differentiate between benign and cancerous lesions of the breast (Garra *et al* 1997, Hall and Zhu 2003). Therefore, ultrasound elastography could conceivably be used to differentiate between conditions in the uterus such as stiff diffuse endometrial carcinoma, soft diffuse endometrial hyperplasia and the softer focal polyps. For example, figure 1 shows an ultrasound B-mode image (left image) of the excised uterus from a 51-year-old hysterectomy patient, along with a corresponding (static) elastogram (right image). The elastogram was created using a two-dimensional block-matching method (Zhu and Hall 2002). Softer tissues appear brighter (white), while stiffer tissue appear darker or towards the black end of the grey scale. The stiffer fibroid is more apparent in the elastogram than in the sonogram since the soft capsule surrounding the fibroid forms a brighter halo around the fibroid. The ability to characterize uterine masses *in vivo* using ultrasound elastography potentially allows the
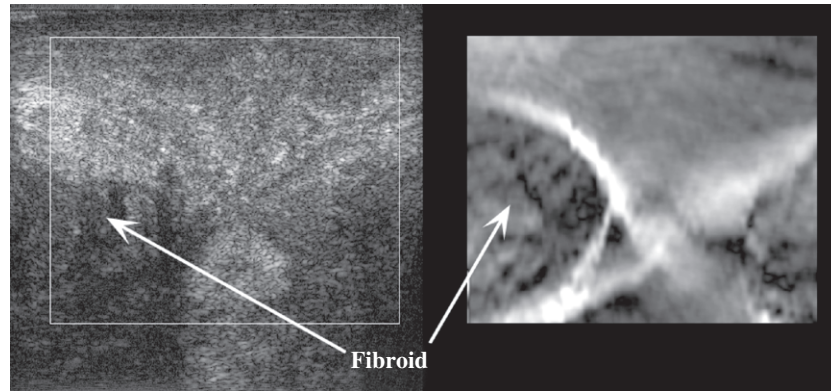
Figure 1. Side-by-side comparison of an ultrasound B-mode image with the corresponding elastogram of an excised uterus from a 51-year-old patient. The width of the B-mode image is 5 cm. The location of the fibroid is indicated by the arrow.

physician to decide on appropriate treatment methods, including non- or minimally invasive alternatives to a hysterectomy.

Determination of the effectiveness of ultrasound elastography to differentiate between the stiffer leiomyomas and softer adenomyosis requires the quantification of the viscoelastic characteristics of the uterus, cervix and associated pathologies to determine the modulus contrast. The true elastic contrast can be then compared to the contrast between normal tissue, leiomyomas and other diffuse and focal masses seen on strain elastograms (Hobson *et al* 2005). In this paper, we report experiments to determine the frequency-dependent complex modulus of excised human uterine tissue, cervical tissue and leiomyomas. The results are presented, and their implications in the development of ultrasound elastography as an imaging modality are discussed.

2. Materials and methods

2.1. Theory

Determination of the complex moduli in excised tissue is a straightforward procedure. Although there are more rigorous treatments in the literature (Christensen 1982, Fung 1993), the basic derivation is summarized here. When a viscoelastic material is deformed (i.e., strain is applied), it responds with some level of stress. Expressed in terms of a Stieltjes integral (Christensen 1982), the stress σ is related to the strain ε (deformation) by the following constitutive relation:

$$\sigma(t) = \int_{-\infty}^{t} E(t - \tau) \frac{d\varepsilon(\tau)}{d\tau} \, d\tau, \tag{1}$$

where the relaxation function, $E(t)$, represents the mechanical properties of the material. For the sake of simplicity, the material is assumed to be linearly viscoelastic and isotropic. If the applied strain or perturbation is periodic,

$$\varepsilon(t) = \varepsilon_0 \, e^{i\omega t}, \tag{2}$$

where ε_0 is the peak-to-peak strain amplitude and ω is the frequency, then the stress response will also be periodic, shifted by some phase angle δ:

$$\sigma(t) = \sigma_0 \, e^{i(\omega t + \delta)}, \tag{3}$$

where σ_0 is the peak-to-peak stress amplitude. Substituting equations (2) and (3) into (1), solving and performing a Fourier transform on the result produces

$$\sigma(\omega) = E^*(\omega)\varepsilon(\omega), \tag{4}$$

where $E^*(\omega)$ is the frequency-dependent complex modulus of the material. Accounting for the phase shift presented in equation (3), $E^*(\omega)$, is expressed as

$$E^*(\omega) = \frac{\sigma_0}{\varepsilon_0}(\cos\delta + i\sin\delta). \tag{5}$$

The real part of equation (5) is known as the storage modulus and reflects the ability of the material to store energy during a loading cycle. The imaginary part is called the loss modulus and indicates the amount of energy lost during each cycle. While the real and imaginary parts can be easily determined, it is more common to present the data in terms of the magnitude and phase, given by $|E^*(\omega)|$ and $\tan\delta$, respectively.

When a strain elastogram is constructed, one quantity of interest to researchers is the strain contrast between the normal uterine tissue and associated pathologies. Strain contrast has been shown to correlate with modulus contrast (Kallel *et al* 1996, Ophir *et al* 1997, Srinivasan *et al* 2002), which is defined as the ratio of the modulus of an inclusion to that of the surrounding normal tissue. In the case of a frequency-dependent complex modulus, this is best represented by

$$C_t^*(\omega) = \frac{E_{\text{fibroid}}^*(\omega)}{E_{\text{uterus}}^*(\omega)}. \tag{6}$$

In general, $C_t^*(\omega)$ is a complex quantity, but it has been shown that the imaginary part is approximately zero (Kiss *et al* 2004). This number therefore is then represented by taking the magnitudes of the two moduli, resulting in a modulus contrast that is real.

2.2. Experiment

Uterine tissue samples from 24 women ranging in age from 31 to 79 were subjected to a series of dynamic tests using the EnduraTEC ELF 3220 (Bose Corporation, EnduraTEC Systems Group, Minnetonka, MN, USA) test system in order to determine their viscoelastic properties. This study was approved by the University of Wisconsin Institutional Review Board. Patient consent was obtained for the mechanical testing of the excised tissue. Each patient had been diagnosed with a pathology necessitating a compete hysterectomy, requiring removal of the entire uterus. All surgical procedures were performed at the University of Wisconsin hospital in Madison, Wisconsin. Following surgical resection, the entire organ was transferred to the Surgical Pathology facility. Rectangular specimens typically 25 mm on a side and approximately 5 mm thick were excised from the uterine and cervical walls by a pathologist and placed in water and transported to our laboratory for mechanical testing. Samples were tested typically within 2 h of the organ being transferred to the Surgical Pathology facility. The specimens were kept in a refrigerator and allowed to come to room temperature for testing. The specimens were further cut to rectangular slabs 10–20 mm on a side to minimize thickness nonuniformity. All dimensions were measured several times using a pair of dial callipers, and the results were averaged. From each patient, a part of the cervix and two orthogonally oriented sections of the uterine wall were obtained. In the uterine samples, the muscle fibres generally ran either perpendicular or parallel to the short axis of the sample. Throughout this project, these are denoted by the terms uterus $\perp$ and uterus $\parallel$, respectively. The same was not done with cervical tissue due to the limited amounts of material that could be obtained from the intact cervix. But the fibres in the cervical tissue samples generally ran perpendicular
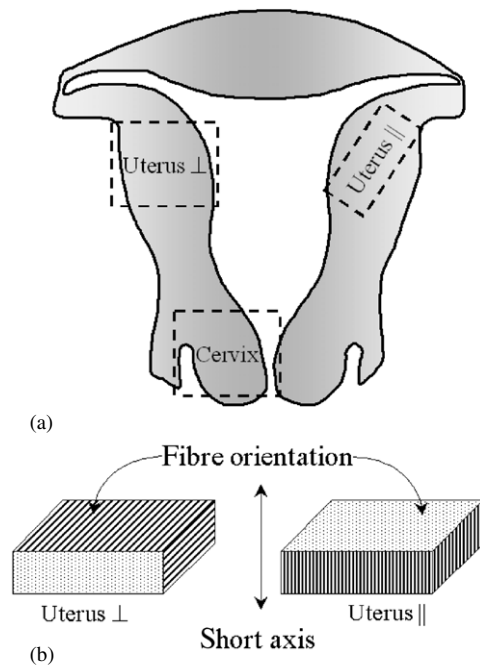
Figure 2. Schematic of the uterus. The drawings are illustrative and are not to scale. (a) Uterus and cervix showing the typical location of the tissue samples. (b) Schematic of the uterine tissue samples showing the general orientation of the fibres in the uterus specimens. Uterus ⊥ is on the left and uterus ∥ is on the right.

to the shortest axis of the sample. Leiomyoma fibroids were obtained when available in the uterine tissue. The leiomyomas had no distinct fibre orientation. Figure 2 is a schematic of the uterus showing the locations from which each sample (cervix and uterus only) was obtained. The mean patient age was 50.4 ± 10.8 year.

Using the ELF 3220, the samples were subjected to periodic strain in the frequency range from 0.1 to 100 Hz and under three amplitude ranges 1–2%, 2–3% and 2–4%. The first number in the range is the minimum strain the sample was subjected to, and the second number is the maximum strain. Therefore, the corresponding strain amplitudes (peak to peak) for each of these cases are 1%, 1% and 2%, respectively. Amplitudes and ranges were all kept low because it had been determined through trial and error that maximum compressions greater than 5% exhibited nonlinear results and minimum compressions less than 1% did not ensure uniform deformation of the sample. Table 1 summarizes the number of samples tested for each component and shows the number of samples tested in each frequency range. The difference in the number of samples tested for each component differs due to viability of that component as determined by the pathologist. For example, in the case of one patient, no normal uterine tissue was obtained because the uterus was profuse with leiomyomas.

Samples and the contact surfaces were coated with a thin film mineral oil prior to testing. The thin film on the sample minimized sample desiccation and promoted free slip conditions between it and the ELF contact surfaces. As each sample was placed onto the load cell of the ELF, the system was zeroed out to establish the contact point between the ELF and the sample. The system was controlled using the ELF dynamic mechanical analysis (DMA) software, compressing the sample at a specified amplitude and frequency. For each amplitude range,
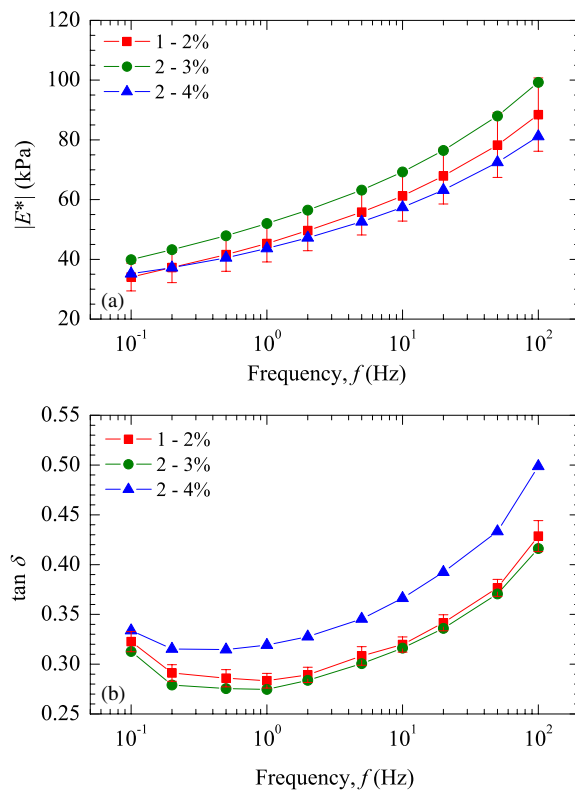
Figure 3. Experimental results for cervical tissue for three compression ranges, displayed in terms of the pre-compression and compression amplitude: (a) magnitude of the complex modulus and (b) tan δ.

Table 1. Summary of specimens obtained.

Component	Frequency range (%)	Number of samples tested
Cervix	1–2	24
	2–3	24
	2–4	24
Uterus ⊥	1–2	22
	2–3	24
	2–4	23
Uterus ∥	1–2	17
	2–3	17
	2–4	17
Leiomyoma	1–2	7
	2–3	8
	2–4	7

the system was allowed to vibrate at the selected frequency for up to 10 s to allow the system to achieve equilibrium, to allow transients to decay and to allow the sample to precondition (Fung 1993). The time between acquiring data at any two frequencies was 5 s, at which point
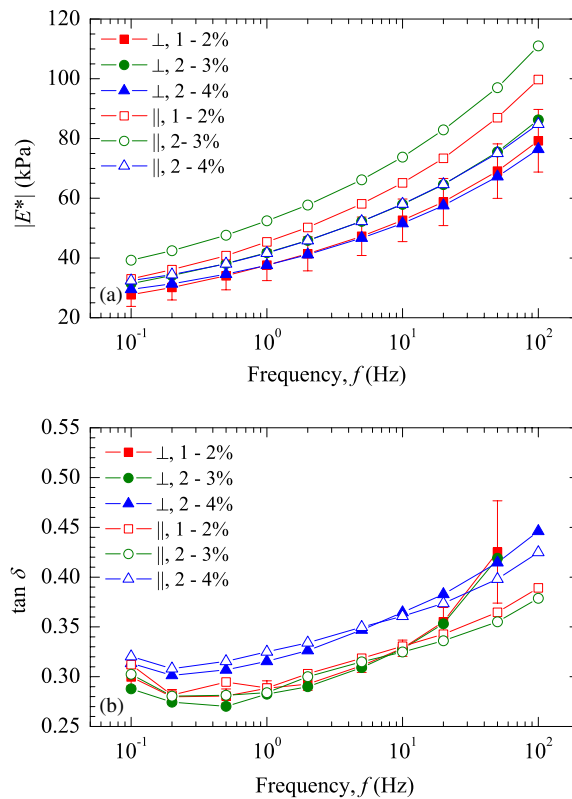
Figure 4. Results for uterus ⊥ and uterus ∥ for three compression conditions: (a) magnitude of the complex modulus and (b) tan δ.

the sample was held at the mean strain level (1.5%, 2.5% and 3%, respectively). This was done to allow the tissue to relax prior to a subsequent test. The output from the DMA software includes $|E^*(f)|$, $E''(f)$, $E(f)$ and tan δ, where f is the testing frequency and is related to ω in the above equations as $\omega = 2\pi f$. The algorithm for calculation is based on the report from ASTM International (2001).

3. Results

$|E^*(f)|$ and tan δ, the frequency-dependent modulus and phase of the cervical tissue are shown in figures 3(a) and (b), respectively. Error bars represent the standard error of the mean and are shown for the 1–2% amplitude range. From 0.1–to 100 Hz, the modulus monotonically increases from 33 kPa to more than 95 kPa in this tissue. The 2–3% amplitude range results in the highest moduli over all frequencies tested when compared with the 1–2% and 2–4% ranges, with a difference of approximately 6 kPa at 0.1 Hz up to a difference of as much as 18 kPa at 100 Hz. The differences in the moduli between all these three amplitude ranges tend to increase with increasing mechanical loading frequency. In the case of the phase results in figure 3(b), all three cases initially decrease to a minimum around 0.275–0.320 near 1.0 Hz, and then increase to their maximum values from 0.42 to 0.50 at 100 Hz. The 2–4% amplitude range possesses the highest tan δ over all the frequencies tested.
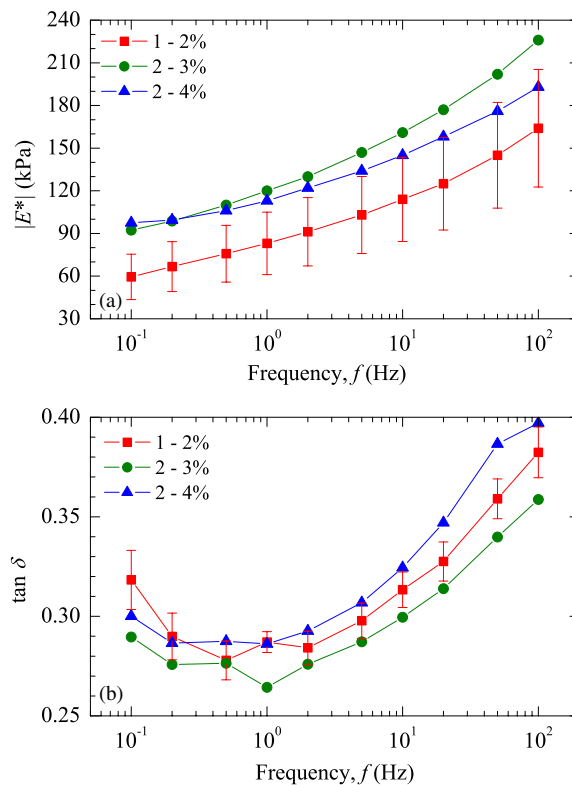
Figure 5. Results for leiomyoma for three compression conditions: (a) magnitude of the complex modulus and (b) tan δ.

Figure 4 shows the frequency-dependent modulus and phase results for both the uterus $\perp$ and uterus $\parallel$ cases. The uterus $\parallel$ has a higher modulus than the uterus $\perp$ over all frequencies tested and for all three amplitude ranges. Values for the modulus range from 28–35 kPa at 0.1 Hz up to 78–95 kPa at 100 Hz. The uterus $\parallel$ at 2–3% has the highest modulus overall compared to all other uterine cases in this figure. However, the values tend not to spread out as the frequency increases, unlike the case for the cervix, shown in figure 3(a). The values keep a roughly constant difference throughout the entire range of frequencies. The tan δ values in figure 4(b) show a similar behaviour as that of the cervix and also lie within the same range of values.

The frequency-dependent modulus and phase results for the leiomyomas are shown in figure 5. The large error bars in figure 5(a) are due to the fact that only eight samples were averaged to estimate the mean and standard error of the mean. The moduli of the leiomyomas are significantly higher than either those of the cervix or the uterus. In fact, the graph has a much broader vertical scale than either figure 3(a) or 4(a), so direct comparison is limited between it and figure 3(a) or 4(a). The moduli range from 60–95 kPa at 0.1 Hz up to 175–225 kPa at 100 Hz. In this case, unlike the cervix and normal uterus, the 1–2% range has the highest moduli over all frequencies tested. The tan δ values shown in figure 6(b) resemble, both in behaviour and value, the results in figures 4(b) and 5(b).

A direct comparison of the four tissue types is shown in figure 6, for the 2–3% strain range. From figure 6(a) the modulus of the fibroid is roughly three times larger than that of
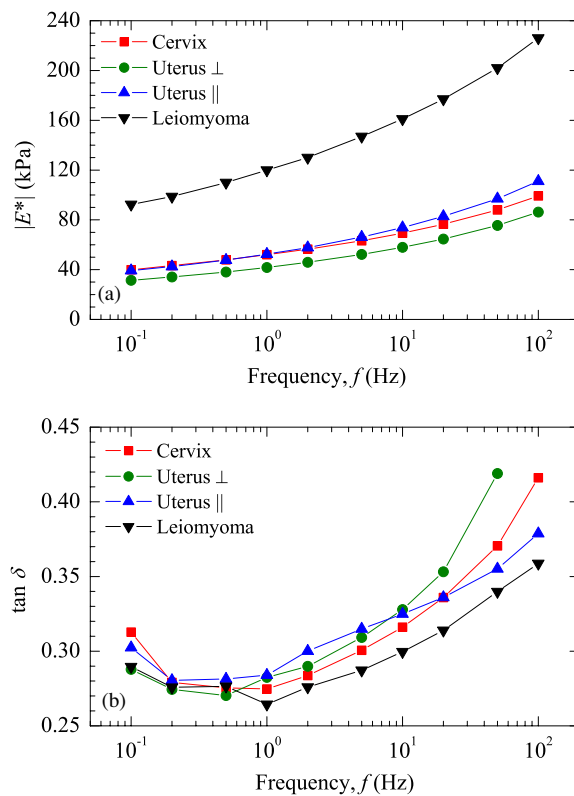
Figure 6. Comparison of the four tissue types (cervix, uterus ⊥, uterus ∥ and leiomyoma) for the 2–3% condition as a function of frequency: (a) magnitude of the complex modulus and (b) tan δ.

all normal tissues at 0.1 Hz, and a little more than twice as large at 100 Hz. The normal tissue values all reside in a small vertical range of values and are similar. Error bars have been left out here for clarity, and the reader is directed to the previous figures to get an idea of their ranges. The tissue types possess very similar tan δ values, as shown in figure 6(b), but only up to about 10 Hz, above which the values spread, particularly for the uterus ⊥ case, as the frequency increases. It is possible that at high frequencies (>20 Hz) experimental artefacts contaminated some data sets.

4. Discussion

The frequency-dependent complex modulus of uterine tissue has been characterized here for a range of small strain amplitudes and low pre-compression strain ranges. As shown in figures 3–6, the cervix, uterus and leiomyoma all have moduli that are directly proportional to frequency. It is tempting to compare these results using conventional viscoelastic models, such as those discussed in Fung (1993). However, several authors (Suki *et al* 1994, Taylor *et al* 2001, 2002, 2003, Nasseri and Bilston 2002, Chen *et al* 2003, Kiss *et al* 2004) have demonstrated that the conventional constitutive relations (i.e., Kelvin–Voigt model, the Maxwell model or the standard linear solid model) do not correctly or completely model the behaviour seen empirically, and the results are better correlated with some sort of power law.
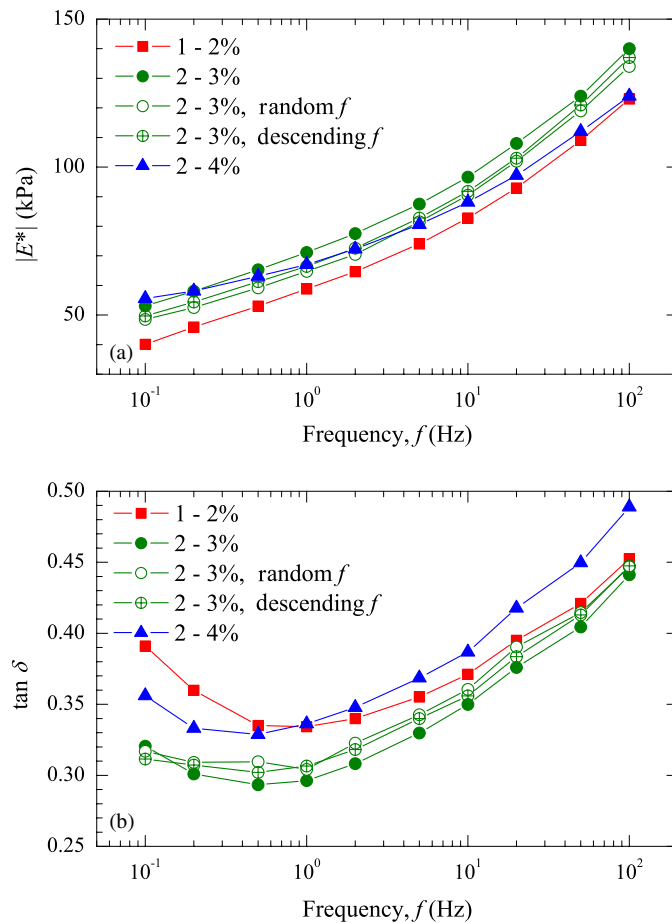
Figure 7. Results for a single uterus ‖ sample in which the order of testing has been reversed from the conventional protocol. The 2–4% range was tested first, followed by the 2–3% and 1–2% ranges. Additionally, for the 2–3% case, results are shown for three frequency strategies: sequentially increased testing frequency, sequentially decreased testing frequency and randomly selected order of testing frequency: (a) magnitude of the complex modulus and (b) tan δ.

Although no attempt has been made here to compare the results to actual power law behaviour, the behaviour of the modulus as a function of frequency suggests a good correlation.

In a direct comparison of the moduli of the various tissue types, as shown in figure 6(a), it is clear that the leiomyoma is much stiffer than normal uterine or cervical tissue. It is still apparent that the cervix and uterus have statistically similar modulus values. This similarity results from averaging the moduli values over all patients. In individual patients, cervical tissue may be stiffer than uterine tissue, or vice versa, but the conditions determining the case have not been fully characterized, and are beyond the scope of this paper. Further studies are warranted to determine these characteristics, which may include the dependence on age, number or children, or menopausal status. It is notable that the important factor in lesion detection is the variation in the modulus of the lesion compared to that of the uterus.

The phase information of the various components all behave similarly over the range of frequencies tested. In the direct comparison shown in figure 6(b), there is little variation between the tissue types. The cause of the local minimum in tan δ between 0.1 and 1.0 Hz is
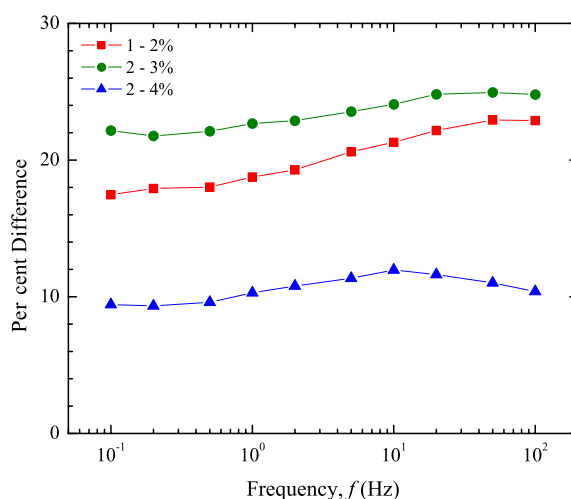
Figure 8. Per cent difference in moduli values between uterus ⊥ and uterus ∥ for three compression ranges.

not entirely clear, and is the subject of ongoing investigations. As all tissue types have roughly the same value for tan δ at any given frequency, this may be a property of some muscle tissue. On the other hand, in tissue such as the liver, tan δ increased monotonically with frequency (Kiss *et al* 2004).

To eliminate possible experimental bias, some samples were tested by varying the order of the strain protocols, or the testing frequency (either by starting at 100 Hz and sequentially testing decreasing frequencies, or by randomly choosing the frequency sequence). In each case, the phase was non-monotonic. Figure 7 shows a plot of one such sample. In this case, the 2–4% range was tested first, followed by the 2–3% and the 1–2%. Two additional cases for the 2–3% range were tested, in which the testing frequency was sequentially decreased from 100 to 0.1 Hz, and in which the order of the testing frequency was randomly selected. Figure 7(a) shows that the modulus, while stiffer than the average values presented in figure 4(a), preserves the same features. This is also the case in figure 7(b) for tan δ.

One of the dividends of this study is that it may let researchers estimate the expected strain contrast from an axial strain image, which is an important requirement in the development of cervical and uterine elastography (Hobson *et al* 2005). Strain contrast depends in part on the modulus contrast. In general, the modulus values of leiomyoma samples was greater than those of normal uterine tissue, with a mean contrast at 1 Hz of 3.75 ± 1.4 (based on six patients from which uterus ⊥ and fibroid data exist, and for the 2–3% range), where contrast is taken as the ratio of the modulus of the leiomyoma to that of the uterus (as in equation (6)). In these preliminary data, there also appears to be some variability in the contrast among the different samples tested, as indicated by the large standard error of the individual contrast measures. In fact, for one of the six samples, the modulus of the fibroid was lower than that of the normal tissue, a rather surprising finding given the perception that these tumours are stiff and easily palpable. These preliminary data are intended to be used as a guide for further studies of elastic moduli on fibroids as well as other tumours in the uterus.

A quantitative comparison of the uterus ∥ and uterus ⊥ tissues is shown in figure 8, with the per cent difference of the mean values of the magnitude of the modulus plotted as a function of the frequency for the three compression protocols. The modulus showed the

smallest difference in the 2–4% range, with values in the vicinity of 10% across the range of frequencies. In the 1–2% case, the percent difference steadily increased from 19% at 0.1 Hz up to 21% at 100 Hz, and in the 2–3% case, the values were in the vicinity of 21% with a slight increase over the range of frequencies.

5. Conclusion

Viscoelastic properties of uterine tissue have been measured. The results reported here show that the moduli of the cervix, the uterus and associated uterine fibroids are both frequency and strain amplitude dependent. These results demonstrate the potential for developing elastography as a method of diagnosing and monitoring diseases of the uterus. The emphasis here has been on the general dependence of the modulus on testing frequency. Future investigations will focus on the relationship between the modulus to patient age, history of cancer and number of children, as well as incorporating these results into a uterine elastography model.

Acknowledgments

References

Ascher S M, Jha R C and Reinhold C 2003 Adenomyosis: MRI of the uterus treated with uterine artery embolization *Top. Magn. Reson. Imaging* **14** 281–304
ASTM International 2001 *Standard Guide for Dynamic Testing of Vulcanized Rubber and Rubber-Like Materials Using Vibratory Methods*, D5992-96
Bazot M, Cortez A, Darai E, Rouger J, Chopier J, Antoine J M and Uzan S 2001 Ultrasonography compared with magnetic resonance imaging for the diagnosis of adenomyosis: correlation with histopathology *Hum. Reprod.* **16** 2427–33
Berridge D L and Winter T C 2004 Saline infusion sonohysterography: technique, indications, and imaging findings *J. Ultrasound Med.* **23** 97–112
Bhatia K G and Singh V R 2001 Ultrasonic characteristics of leiomyoma uteri *in vitro Ultrasound Med Biol* **27** 983–7
Bree R L, Bowerman R A, Bohm-Velez M, Benson C B, Doubilet P M, DeDreu S and Punch M R 2000 US evaluations of the uterus in patients with postmenopausal bleeding: a positive effect on diagnostic decision making *Radiology* **216** 260–4
Caoili E M, Hertzberg B S, Kliewer M A, DeLong D and Bowie J D 2000 Refractory shadowing from pelvic masses on sonography: a useful diagnostic sign for uterine leiomyomas *Am. J. Roentgenol.* **174** 97–101
Chen Q, Suki B and An K N 2003 Dynamical mechanical properties of agarose gel by a fractional derivative model *2003 Summer Bioengineering Conf. (Key Biscayne, FL 2003)* ed L J Soslowsky
Christensen R M 1982 *Theory of Viscoelasticity: An Introduction* (New York: Academic)
Davidson K G and Dubinsky T J 2003 Ultrasonographic evaluation of the endometrium in postmenopausal vaginal bleeding *Radiol. Clin. North Am.* **41** 769–80
Devlieger R, D'Hooghe T and Timmerman D 2003 Uterine adenomyosis in the infertility clinic *Hum. Reprod. Update* **9** 139–47
Fung Y C 1993 *Biomechanics* (New York: Springer)
Garra B-S, Cespedes E I, Ophir J, Spratt S R, Zuurbier R A, Magnant C M and Pennanen M F 1997 Elastography of breast lesions: initial clinical results *Radiology* **202** 79–86
Hall T J and Zhu Y 2003 *In vivo* real-time freehand palpation imaging *Ultrasound Med. Biol.* **29** 427–35
Hobson M A, Kiss M Z, Shi H, Varghese T, Kliewer M A, Zagzebski J A, Hall T J, Harter J, Hartenbach E M and Madsen E L 2005 Uterine elastography *J. Ultrasound. Med.* **24** S85

Kallel F, Bertrand M and Ophir J 1996 Fundamental limitations on the contrast-transfer efficiency in elastography: an analytic study *Ultrasound Med. Biol.* **22** 463–70

Keshavarzi A, Vaezy S, Kaczkowski P J, Keilman G, Martin R, Chi E Y, Garcia R and Fujimoto V Y 2001 Attenuation coefficient and sound speed in human myometrium and uterine fibroid tumors *J. Ultrasound Med.* **20** 473–80

Kiss M Z, Varghese T and Hall T J 2004 Viscoelastic characterization of *in vitro* canine tissue *Phys. Med. Biol.* **49** 4207–18

Kliewer M A, Hertzberg B S, George P Y, McDonald J W, Bowie J D and Carroll B A 1995 Acoustic shadowing from uterine leiomyomas-sonographic-pathological correlation *Radiology* **196** 99–102

Nasseri S and Bilston L E 2002 Viscoelastic properties of pig kidney in shear, experimental results and modeling *Rheol. Acta* **41** 180–92

Ophir J, Kallel F, Varghese T, Bertrand M, Cespedes I and Ponnekanti H 1997 Elastography: a systems approach *Int. J. Imaging Syst. Technol.* **8** 89–103

Reinhold C, McCarthy S, Bret P M, Mehio A, Atri M, Zakarian R, Glaude Y, Liang L J and Seymour R J 1996 Diffuse adenomyosis: comparison of endovaginal US and MR imaging with histopathologic correlation *Radiology* **199** 151–8

Reinhold C, Tafazoli F, Mehio A, Wang L, Atri M, Siegelman E S and Rohoman L 1999 Uterine adenomyosis: endovaginal US and MR imaging features with histopathologic correlation *Radiographics* **19** S147–S60

Srinivasan S, Ophir J and Alam S K 2002 Elastographic imaging using staggered strain estimates *Ultrason. Imaging* **24** 229–45

Suki B, Barabási A-L and Lutchen K R 1994 Lung tissue viscoelasticity: a mathematical framework and its molecular basis *J. Appl. Physiol.* **76** 2749–59

Takeuchi M, Matsuzaki K, Yoshida S and Nishitani H 2005 Pathologies of the uterine endometrial cavity: usual and unusual manifestations and pitfalls on magnetic resonance imaging *Eur. Radiol.* **15** 2244–55

Taylor L S, Lerner A L, Rubens D J and Parker K J 2002 A Kelvin–Voigt fractional derivative model for viscoelastic characterization of liver tissue *2002 ASME International Mechanical Engineering Congress and Exposition (New Orleans, LA)* ed E P Scott (New York: ASME International)

Taylor L S, Richards M S, Moskowitz A J, Lerner A L, Rubens D J and Parker K J 2001 Viscoelastic effects in sonoelastography: impact on tumor detectability *2001 IEEE Ultrasonics Symp.* pp 1639–42

Taylor L S, Rubens D J, Mejia L and Parker K J 2003 Preliminary results of cyclic uniaxial compression of bovine liver *2003 ASME International Mechanical Engineering Congress and Exposition (Washington, D.C.)*

Williams P L, Laifer-Narin S L and Ragavendra N 2003 US of abnormal uterine bleeding *Radiographics* **23** 703–18

Wood C 1998 Surgical and medical treatment of adenomyosis *Hum. Reprod. Update* **4** 323–6

Zhu Y and Hall T J 2002 A modified block matching method for real-time freehand strain imaging *Ultrason. Imaging* **24** 161–76